1
2
3
4   Urban-rural interactions govern ozone and oxygenated volatile
5   organic compound formation in a South Korean forest
6

7   [1]Saewung Kim, [2]So-Young Kim, [3]Meehye Lee, [3]Heeyoun Shim,
8   [4,5]Glenn M. Wolfe, [6]Alex B. Guenther, and [1]Amy He, [2]Youdeog Hong,
9   [2]Jinseok Han
10
11
12
13
14
15   1 Department of Earth System Science, School of Physical Sciences, University
16   of California, Irvine, Irvine California, 92697 U.S.A.
17   2 National Institute Environmental Research, Incheon, South Korea
18   3 Department of Earth and Environmental Sciences, Korean University, Seoul,
19   South Korea
20   4 Joint Center for Earth Systems Technology, University of Maryland Baltimore
21   County, Baltimore, MD, USA
22   5 Atmospheric Chemistry and Dynamics Laboratory, NASA Goddard Space
23   Flight Center, Greenbelt, MD, USA
24   6 Atmospheric Sciences and Global Change Division, Pacific Northwest National
25   Laboratory, Richland WA USA
26
27
28
29
30
31
32
33
34
35
36
37
38
39
40
41
42

Abstract

Rapid urbanization and economic development in East Asia in past decades has led to photochemical air pollution problems such as excess photochemical ozone and aerosol formation. Asian megacities such as Seoul, Tokyo, Shanghai, Gangzhou, and Beijing are surrounded by densely forested areas and recent research has consistently demonstrated the importance of biogenic volatile organic compounds (VOCs) from vegetation in determining oxidation capacity in the suburban Asian megacity regions. Uncertainties in constraining tropospheric oxidation capacity, dominated by hydroxyl radical, undermine our ability to assess regional photochemical air pollution problems. We present an observational dataset of CO, NO_X, SO_2, ozone, HONO, and VOCs (anthropogenic and biogenic) from Taehwa Research Forest (TRF) near the Seoul Metropolitan Area (SMA) in early June 2012. The data show that TRF is influenced both by aged pollution and fresh BVOC emissions. With the dataset, we diagnose HOx (OH, HO_2, and RO_2) distributions calculated using the University of Washington Chemical Box Model (UWCM v 2.1) with near-explicit VOC oxidation mechanisms from MCM 3.2 (The Master Chemical Mechanism). Uncertainty from unconstrained HONO sources and radical recycling processes highlighted in recent studies is examined using multiple model simulations with different model constraints. The results suggest that 1) different model simulation scenarios cause systematic differences in HO_X distributions especially OH levels (up to 2.5 times) and 2) radical destruction (HO_2+HO_2 or HO_2+RO_2) could be more efficient than radical recycling (RO_2+NO) especially in the afternoon. Implications of the uncertainties in radical chemistry are discussed with respect to ozone-VOC-NO_X sensitivity and VOC oxidation product formation rates. Overall, the NO_X limited regime

68   is assessed except for the morning hours (8 am to 12 pm) but the degree of sensitivity can

69   significantly vary depending on the model scenarios. The model results also suggest that

70   RO_2 levels are positively correlated with oxygenated VOCs (OVOCs) production that is

71   not routinely constrained by observations. These unconstrained OVOCs can cause higher

72   than expected OH loss rates (missing OH reactivity) and secondary organic aerosol

73   formation. The series of modeling experiments constrained by observations strongly urge

74   observational constraint of the radical pool to enable precise understanding of regional

75   photochemical pollution problems in the East Asian megacity region.

76   1. **Introduction**

77   NOx (NO+NO$_2$) and volatile organic compounds (VOCs) are two important

78   precursors that drive HOx radical cycles(Levy, 1971). In the presence of NO$_X$, VOC

79   oxidation processes recycle OH and produce photochemical oxidation products such as

80   ozone and oxygenated VOCs (OVOCs). This reaction cycle is highly non-linear. For

81   example, excess NO$_2$ may expedite nitric acid formation (R1), limiting ozone production.

82   In the same context, excess VOCs may expedite peroxy radical production (R2), which

83   limits OH regeneration from peroxy radicals.

84

85   OH + NO$_2$ + M ➜ HNO$_3$ + M (R1)

86   HO$_2$ +RO$_2$ ➜ ROOH (R2)

87

88   The non-linearity in tropospheric photochemistry has been relatively well studied

89   in the urban regions of developed countries and applied in ozone reduction policy. The

90   Los Angeles Metropolitan Area has accomplished significant ozone reduction by

91   implementing aggressive emission reductions of both NOx and VOC especially from

92   mobile sources (Ryerson et al., 2013). The remarkable ozone abatement was possible due

93   to the fact that there is no significant pollution transport from other metropolitan areas

94   and no significant natural emission sources especially volatile organic compounds from

95   vegetation (BVOCs; biogenic volatile organic compounds) compared with anthropogenic

96   VOC mostly from mobile sources (Pollack et al., 2013;Huang et al., 2013). In the late 80s,

97   Trainer et al. (1987) first demonstrated the importance of isoprene (C$_5$H$_8$) as a peroxy

98   radical source that can contribute significant ozone production in rural areas. The

99   importance of isoprene in ozone production in urban areas has also been highlighted, e.g.

100   in the Atlanta Metropolitan Area (Chameides et al., 1988).

101   Isoprene is a hemiterpenoid species and is the globally dominant VOC emission

102   from vegetation (Arneth et al., 2011;Guenther, 2013). Arguably, isoprene is the most

103   frequently studied BVOC from the perspective of atmospheric oxidation processes and

104   their implications for ozone and aerosol formation. However, significant uncertainty

105   hinders assessing the roles of isoprene in regional and global photochemistry in three

106   fronts. First, there is still significant uncertainty in estimating emission rates from each

107   individual plant species on regional scales (Guenther, 2013). Second, limited isoprene

108   inter-comparison results (Barket et al., 2001) suggest that there are large systematic

109   biases among different analytical techniques. Lastly, recent laboratory, theoretical and

110   field observations suggest significant uncertainty in tropospheric isoprene oxidation

111   processes initiated by OH. Until early 2000, it was thought that three first generation

112   isoprene oxidation products (methyl vinyl ketone, methacrolein, and formaldehyde) from

113   OH oxidation were enough to constrain isoprene tropospheric oxidation processes for

114   modeling purposes (e.g. Spaulding et al. (2003) and Dreyfus et al. (2002)). This is an

115   interesting evolution of thoughts considering that Paulson and Seinfeld (1992), one of

116   pioneering works describing isoprene oxidation, clearly claimed that 22 % of first

117   generation isoprene oxidation products from the reaction with OH was not identified and

118   likely included multifunctional C5 compounds. Recent advances in analytical techniques

119   (Kim et al., 2013a) have shown that indeed significant C5-hydroxy carbonyl (e.g.

120   isoprene hydroperxyenals, HPALD) and peroxide compounds are produced as first

121   generation isoprene oxidation products (Crounse et al., 2011;Paulot et al., 2009;Wolfe et

122 al., 2012;Zhao and Zhang, 2004). The product yields appeared to be a strong function of

123 NO concentrations (Peeters and Muller, 2010). In general, at low to intermediate NO

124 levels (~ 100 pptv or lower), the yields of C5-hydroxy carbonyl compounds become

125 higher. These new findings in the isoprene oxidation process are also closely related with

126 recent findings in unexpectedly high OH concentrations (Hofzumahaus et al.,

127 2009;Lelieveld et al., 2008) and substantial missing OH sinks also known as

128 unexpectedly high OH reactivity in high isoprene environments (Di Carlo et al.,

129 2004;Edwards et al., 2013;Kim et al., 2011;Lou et al., 2010).

130   These new findings have significant implications for regional air quality

131 especially regarding photochemical ozone and SOA production. Despite the strong

132 anthropogenic pollutant emissions in East Asia (China, Japan and South Korea), recent

133 research has shown that isoprene accounts for a major OH chemical sink in suburban

134 areas near Beijing (Ran et al., 2011), the Pearl River Delta region (Lu et al., 2012), Taipei

135 (Chang et al., 2014) and Seoul (Kim et al., 2013d;Kim et al., 2013b). Consequently,

136 modeling studies also clearly show that isoprene contributes significantly to ozone

137 formation in Asian megacity regions. Kim et al. (2013d) reported that simulated ozone

138 levels with isoprene chemistry are up to 30 % higher than ozone simulation without

139 isoprene chemistry using the WRF-Chem model, indicating an urgent need to implement

140 improved isoprene chemistry schemes in these models in order to simulate the

141 unexpected higher levels of OH in isoprene rich environments. This could become an

142 especially serious issue as Hofzumahaus et al. (2009) reported significantly higher (~ 2.6

143 times at noon) than expected OH levels in the Pearl River Delta region in China.

144 Therefore, the current assessments based on the conventional OH photochemistry could

145   significantly misdiagnose regional air-quality status and mislead policy implementation

146   to reduce photochemical air pollution in the East Asian region. Furthermore, as the

147   importance of BVOC in regional air-quality issues in ozone and SOA formation has been

148   also highlighted in Europe and North America, the uncertainty in isoprene

149   photochemistry has significant implications in urban and suburban air quality in general

150   (Zhang et al., 2008a;Sartelet et al., 2012).

151   We present atmospheric observations of NO_X, CO, VOCs, ozone, and HONO in

152   the Taehwa Research Forest (TRF) in the Seoul Metropolitan Area (SMA), South Korea.

153   We use observed data from June, 2013 to conduct observationally constrained box model

154   (University of Washington Chemical Box Model; UWCM) calculations to estimate OH,

155   HO_2 and RO_2 concentrations with different sets of observational parameters. We discuss

156   current uncertainty in OH-isoprene photochemistry with perspectives of constraining

157   photochemical ozone production and OVOCs precursors of secondary organic aerosols.

158

159   2. **Methods**

160   The Taehwa Research Forest (TRF) is located ~ 35 km from the center of Seoul,

161   South Korea. The TRF is located at the southeastern edge of the Seoul metropolitan Area

162   (SMA, population of ~ 23 million). TRF has a sampling tower located in the middle of a

163   coniferous tree plantation (200 m by 200 m) with the canopy height of 18 m (*Pinus*

164   *koraiensis*) surrounded by a deciduous forest mostly composed by oak. The TRF

165   instrumentation has previously been described by Kim et al. (2013d) along with the

166   previous trace gas observational results. Therefore, just brief descriptions of analytical

167   techniques are given in this paper.

168

2.1. CO, NO_X, SO_2, ozone, VOCs, and meteorological parameters

Thermo Fisher Scientific Enhanced Trace Level Gas Analyzers are used for CO, NO_X, SO_2, and ozone observations as summarized Table 1. A molybdenum (Mo) converter is used to convert NO_2 to NO for the NO_X analyzer. Although Mo converters are still widely used for NO_2 observations, some of thermally unstable oxygenated reactive nitrogen compounds, especially peroxyacyl nitrates, could be also converted to NO_2 by a Mo-converter (Villena et al., 2012). VOC observations are conducted by a High-Sensitivity Proton Transfer Reaction-Mass Spectrometer (PTR-MS, Ionicon GmbH). The atmospheric application of this technique is thoroughly reviewed by de Gouw and Warneke (2007). In addition, the instrument suite at TRF is thoroughly described in (Kim et al., 2013d). PTR-MS can quantify atmospheric VOCs that have higher proton affinity than the proton affinity of H_2O (691 kJ mol^{-1}). Most alkanes have lower proton affinity than water but alkene, aromatic and some OVOCs have higher proton affinity and are suitable for quantification using PTR-MS (Blake et al., 2009). These compounds are more reactive than alkane compounds so PTR-MS has capability to observe reactive atmospheric compounds. The TRF PTR-MS system was set to measure acetaldehyde, acetone, acetic acid, isoprene, methylvinylketone (MVK) + methacrolein (MACR), MEK, benzene, xylene (*p*, *m*, and *o*), and monoterpenes (MT). Each compound was set to be monitored for 1 second each resulting in a sample cycle of 15 seconds. Lower detection limits for the observed VOCs are estimated to be 20 ppt for a 5 second integration with sensitivity of 70 counts ppb^{-1} (2 σ). The uncertainty is estimated as 12 % (2 σ) for the same integration time. Meteorological parameters such as temperature and

191   humidity are monitored by LSI LASTEM Meteorological Sensors. All the presented data

192   is from the 15 m (the canopy height is 18 m) sampling line and meteorological sensors

193   collocated at this height too.

194   PTR-MS with a quadrupole mass filter has an intrinsic limitation that isobaric

195   compounds are all collectively quantified with the same channel (m/z) with a resolution

196   of unit mass. This limitation particularly becomes an issue for investigating the roles of

197   different isomers of MT and sesquiterpenes (SQTs) in photochemistry. For this reason,

198   we also occasionally collect sorbent cartridge samples to analyze MT and SQT speciation

199   in both ambient air and branch enclosure emissions near the sampling tower. As

200   described in (Kim et al., 2013d), Tenax GR and Carbotrap 5TD packed sorbent cartridges

201   (Markes Int, Llanstrisant, UK) were used for sampling. The sampled cartridges were

202   shipped to National Center for Atmospheric Research (NCAR), Boulder CO, USA for

203   gas chromatography-mass spectrometer (GC-MS) analysis. An Agilent 7890 GC/5975 C

204   Electron Impact Mass Spectrometer (GC-MS/FID) in conjunction with a MARKES

205   Unity1/Ultra thermal desorption system optimized for terpenoid analysis quantifies

206   speciated MT and SQT in the sorbent samples. Cartridge samples are both collected from

207   ambient and branch enclosure air. Ambient samples were collected in the mid-day to

208   early afternoon with a volume of 6 L. Ozone in the ambient air was removed using a

209   Na_2SO_3 filter. Branch enclosure samples were also collected, mostly in the mid-day time

210   frame, with a volume of 1 L without an ozone filter as zero air was introduced to the

211   branch enclosure. To explore the diurnal differences in BVOC emissions, branch

212   enclosure samplings were conducted every two hours for three consecutive days in mid

213   June of 2013. We present these analytical results from GC-MS analysis limited to the

214   qualification purpose to examine MT and SQT speciation.

215

216   **2.2 HONO quantification**

217   HONO was measured with an ion chromatography (IC) coupled with diffusion

218   scrubber. Air was introduced to diffusion scrubber (Lab solutions Inc., IL, USA) through

219   a 2 m PFA tubing (1/4" i.d.) at 1.5 L m^{-1} using a filtered orifice restrictor (F-950, air

220   logic, WI, USA). Air flowing through diffusion scrubber interfaced with deionized water,

221   into which HONO was extracted. 50 μL of solution was injected into the IC system

222   through a PEEK loop (Rheodyne, WA, USA) and 6-way valve (EV750-100, Rheodyne,

223   WA, USA). Eluent was a mixture of Na_2CO_3 and $NaHCO_3$, which was pumped by a

224   HPLC pump (DX-100, Dionex, CA, USA) into a guard column (Ionpax® AG 14,

225   4x50mm, Dionex, CA, USA) and then analytical column (Ionpax® AS 14, 4x250mm,

226   Dionex, CA, USA). The column effluent passed through a suppressor (ASRS 300,

227   Dionex, CA, USA) and HONO was detected as nitrite ion in conductivity detector (550,

228   Alltech, IL, USA). The entire measurement processes of sampling, chemical analysis, and

229   data acquisition were controlled by a digital timer and data acquisition software

230   (DSchrom-n, DS science, Korea), by which we obtained two measurements every hour.

231   The system was calibrated using a NO_2^- standard solution (Kanto chemical Co., Inc.,

232   Tokyo, Japan) whenever reagents were replaced. The detection limit was 0.15 ppb

233   estimated from 3σ of the lowest working standard. Specific analytical characteristics are

234   described in Simon and Dasgupta (1995) and Takeuchi et al. (2004).

235

2.3 UWCM box model

236

237   UWCM 2.1 is an open source box model coded by MATLAB (MathWorks®).

238   The model platform can be downloaded from a website

239   (http://sites.google.com/site/wolfegm/code-archive). The box model is embedded its own

240   HO_X (OH+RO_2)-RO_X (peroxyradical and alkoxy radical)-NO_X coupling chemical

241   mechanism. UWCM utilizes Master Chemical Mechanism version 3.2 (MCM 3.2)

242   (Jenkins et al., 1997; Saunders et al., 2003) for near-explicit VOC photo-oxidation

243   schemes. A more detailed model description can be found in Wolfe and Thornton (2011).

244   To minimize uncertainty from the parameterizations of transport and emission, we

245   constrained relatively long-lived trace gases presented in Figure 1. This box modeling

246   technique has been commonly used for examination of OH levels that can be justified by

247   the short chemical lifetime of OH (Kim et al., 2014;Kim et al., 2013c;Mao et al.,

248   2012;Mao et al., 2010). Recently developed isoprene photo-oxidation mechanisms

249   shown in Archibald et al. (2010b) are also incorporated in the model. In addition, Kim et

250   al. (2013c) and Wolfe et al. (2013) applied the model in the identical fashion as used for

251   this study to probe radical distributions using comprehensive observational datasets. This

252   study used the UWCM to simulate the diurnal variations of radical pool (OH+HO_2+RO_2)

253   distributions as observational parameters such as CO, NO_X, ozone, and VOCs are

254   constrained. To fully account for roles of OVOCs in the box model as radical sources, we

255   simulated three consecutive days and presented diurnal variations from the third day. The

256   specific parameters (CO, NO_X, ozone, HONO and VOCs), constrained by

257   observations are described in section 2.1 and 2.2 and presented in Figure 1.

258

259 **3. Results and Discussion**

260 **3.1. Observational Results**

261   Diurnal averages of observed trace gases (June 1st 2012 to June 6th 2012) are

262 shown in Figure 1. The TRF observatory is in continuous operation and we choose this

263 six day period because a regional high-pressure system caused a stagnant air pollution

264 event in this period. In the center of Seoul (the real-time data available at

265 http://www.airkorea.or.kr), carbon monoxide was observed in the similar levels during

266 the focused period (June 1st to June 6th, 2012). On the other hand, the NO_2 level observed

267 in central Seoul was much higher (20-50 ppb) compared with observed levels at TRF.

268 The reason can be attributed to differences between the chemical lifetime of CO (~a

269 month) and NO_2 (~a few hours to a day). The observations clearly indicate that the TRF

270 is not directly influenced by fresh SMA pollution plumes although the TRF is very close

271 to the center of Seoul (30 km away from the city center) as a regional modeling study

272 shows most of CO and NO_X sources are located in the city center (Ryu et al., 2013).

273 Similar observations were also reported for other East Asian megacities such as Beijing

274 (Ma et al., 2012), where ~ 30 ppb and ~ 15 ppb of NO_2 were observed at noon in the

275 urban and the adjacent rural sites, respectively. In contrast, there were no noticeable

276 differences in CO levels between the urban and rural sites (~ 1-2 ppm). The observed

277 CO, NO_X and SO_2 levels in TRF were much lower than those observed in the suburban

278 regions of Chinese megacities such as Beijing (Ma et al., 2012), Shanghai (Tie et al.,

279 2013), and the Pearl River Delta Region (Lu et al., 2012) and similar with the observed

280 levels in Tokyo, Japan (Yoshino et al., 2012).

281   Previous VOC observations in the SMA consistently have shown that toluene is

282   the dominant anthropogenic VOC followed by other aromatic compounds such as xylene

283   and benzene (Kim et al., 2012;Na and Kim, 2001). Na and Kim (2001) reported high

284   concentrations of propane from house hold fuel use. However, recent observation results

285   from the photochemical pollution observational network managed by National Institute of

286   Environmental Research (NIER) of South Korea in the SMA clearly indicate that propane

287   levels have declined and are now much lower than the levels previously observed (NIER,

288   2010). This is probably caused by the implementation of a policy changing household

289   fuel sources from propane to methane. Kim et al. (2012) presented detailed aromatic

290   VOC distributions in the SMA from four different urban observational sites. In average,

291   toluene concentrations were observed ~ 7 times higher than the observed levels of xylene

292   and benzene. At the TRF, a similar anthropogenic VOC speciation distribution was

293   observed as shown in Figure 1. The observed toluene and MEK (methyl ethyl ketone)

294   mixing-ratios were much higher than benzene and xylene. MEK is detected in m/z of 73^+

295   by PTR-MS. Although methyl glyoxal, an atmospheric VOC oxidation product, is also

296   detected on the same mass, we assumed that 73^+ of m/z signals are mostly from MEK, an

297   anthropogenic VOC, since the temporal variation follows that of anthropogenic VOC

298   such as toluene and xylene. In addition, atmospheric lifetime of methyl glyoxal is much

299   shorter than MEK.

300   As the observation facility is located in the middle of a pine tree plantation (*Pinus*

301   *koraiensis*), monoterpenes (MT) are consistently observed. The temporal variation of

302   monoterpenes is affected by the planetary boundary layer evolution with a pattern of

303   higher MT levels during night than those of mid-day as has been often reported in other

304   forest environments (Bryan et al., 2012;Kim et al., 2010) This can be explained by

305   interplays between boundary layer evolution and temperature dependent MT emission. It

306   should also be noted that the continuous branch enclosure BVOC emission observations

307   indicate that the daily maxima of MT and SQT emissions were observed in the midday

308   (between noon to 2 pm in the local time). The observed MT and SQT speciation

309   information in the midday is summarized in Table 2. Table 2a summarizes branch

310   enclosure sample analysis results and ambient sample analysis results are summarized in

311   Table 2b. In general, observed MT and SQT in the ambient air are consistent with

312   previously observed distributions (Kim et al., 2013d). α-pinene and β-pinene were the

313   dominant monoterpene and longifolene was the only detected SQT species. In contrast,

314   the branch enclosure observation results, reflecting BVOC emission, indicate high

315   emission of very reactive MT and SQT species such as β-myrcene, α-caryophyllene, and

316   β-caryophyllene. The fast oxidation of these highly reactive terpenoid species is expected

317   to limit the atmospheric presence of the compounds. Therefore, photochemical oxidation

318   processes of these compounds may have been neglected. Investigating emissions and

319   photochemistry of these reactive terpenoid compounds can constrain potential missing

320   OH reactivity and SOA production from highly oxidized reaction products.

321   Isoprene is produced from carbon recently fixed through photosynthesis resulting

322   in higher emissions and atmospheric concentrations during the daytime. The temporal

323   variation shown in Figure 1 reveals an isoprene concentration maximum between 17:00

324   to 20:00. In addition, the ratios of MVK+MACR, major isoprene oxidation products and

325   isoprene at this period, are significantly lower than those of late morning to early

326   afternoon. The enhanced isoprene levels in the late afternoon or early evening have been

327   also reported in previous studies (Apel et al., 2002;Bryan et al., 2012). The branch

328   enclosure observations demonstrate that isoprene is not emitted from the pine plantation

329   but rather transported from surrounding broadleaf forests as right outside of the pine

330   plantation (200 m × 200 m) is a forested area dominated by oak trees. Oak comprises 85 %

331   of broadleaf trees in South Korea (Lim et al., 2011). Lim et al. (2011) quantified isoprene

332   emission rates for five representative oak species in South Korea and report a wide

333   emission range from oaks that are negligible isoprene emitters (<0.004 $\mu gC\ dw^{-1}\ h^{-1}$;

334   standard emission rates) to others with very high isoprene emission rates of 130 $\mu gC\ dw^{-1}$

335   h^{-1}. It is also noticeable that isoprene is observed in high levels (up to 1 ppb) even during

336   the night. Observational results from the Pearl River Delta region in China also show

337   high isoprene concentration episodes of more than 1 ppb during the night (Lu et al.,

338   2012). As there are some speculations on potential artifacts on isoprene measurements

339   using PTR-MS in environments with large oil and gas evaporative sources (Yuan et al.,

340   2014), the assessments of the potential artifacts should be investigated further in the

341   Asian megacity region.

342   Contributions from each trace gas species towards ambient OH reactivity are

343   shown in Figure 2. This is calculated as the product of the observed species concentration

344   and its rate constant for reaction with OH. Observed OH reactivity from VOCs are much

345   higher than from other trace gases such as CO, NOx, SO_2, and ozone. Among the

346   observed VOC species, BVOCs such as isoprene, α-pinene and β-pinene accounted for

347   significantly higher OH reactivity in comparison with the observed AVOCs such as

348   toluene, benzene, xylene and MEK. Isoprene accounts the highest OH reactivity

349   especially during the daytime. This analysis is consistent with reports from other

350   suburban observations from East Asian megacities such as Beijing (Ran et al., 2011), the

351   PRD region, China (Lou et al., 2010), and the Kinki region Japan (Bao et al., 2010).

352   HONO levels up to 1 ppb were observed in the early morning and were

353   consistently higher than 0.5 ppb during the daytime. These observed levels are

354   substantially higher than reported observations from forest environments in North

355   America (Ren et al., 2011;Zhou et al., 2011), where NO_X (~ 1 ppb) is substantially lower

356   than the level observed at TRF. Ren et al. (2011) reported 30 – 60 ppt of HONO at the

357   Blodgett Forest Research Station in the western foothills of the Sierra Nevada Mountains

358   in the late summer of 2007. Zhou et al. (2011) also reported the similar levels of HONO

359   (below 100 ppt) from the PROPHET forest, a mixed hardwood forest in northern

360   Michigan (Pellston, MI). However, significantly higher HONO levels (~ 200 ppt to ~ 2

361   ppb) were reported by Li et al. (2012) from a rural observational site in the Pearl River

362   Delta region near Guangzhou, where comparable NO_2 levels with TRF were observed.

363   The high HONO levels (a few hundred ppt) especially during the daytime have been

364   consistently reported near Eastern Asian megacities such as Beijing (Li et al., 2012),

365   Shanghai (Hao et al., 2006), and Seoul (Song et al., 2009). Still these are limited datasets

366   and further comprehensive analysis, especially more extensive observation is required.

367   However, two recently proposed HONO production mechanisms may be able to explain

368   the higher levels in the Eastern Asian megacity region. One is HONO production from

369   NO_2 photo-excitation (Wong et al., 2012) as the region usually has high NO_2

370   concentrations and the other is HONO emission from soil bacteria (Oswald et al., 2013).

371   Oswald et al. (2013) found differences as much as two orders of magnitude in HONO

372   emissions from soil samples from different environments (e.g. pH and nutrient contents).

373 In addition, as most of observations in the East Asia regions were conducted with ion

374 chromatography based methods, more direct HONO quantification techniques such as a

375 chemical ionization mass spectrometry technique (Roberts et al., 2010) need to be used to

376 characterize any potential interferences such a high NO_X environment (e.g. N_2O_5).

377

378 **3.2 HO_X Model calculations to examine different isoprene photo-oxidation scenarios**

379 **and the roles of unconstrained HONO sources.**

380 The presented observational results are used to constrain the UWCM box model.

381 We evaluate uncertainties in the tropospheric oxidation capacity and how it affects our

382 ability to constrain ozone and OVOCs production. The observational results clearly

383 indicate that isoprene is the most dominant OH sink among the observed VOCs. In

384 addition, NO concentrations were higher in the 600 to 800 ppt range in the morning. On

385 the other hand, afternoon levels were substantially lower in the 50 to 100 ppt range. The

386 environment provides a unique opportunity to examine implications of isoprene

387 photochemistry in various NO conditions.

388 We conducted model simulation under four different scenarios. Each scenario is

389 described in Table 3. The quantitative assessments of the impacts to radical

390 concentrations (OH, HO_2, and RO_2) from unknown HONO sources are evaluated by

391 examining the outcomes of the model simulations with and without observed HONO. To

392 evaluate the impacts of hydroperoxy-methyl-butenal (HPALD) photolysis and isoprene

393 peroxy radical recycling in the radical pool, each chemical mechanism is selectively

394 constrained by different scenarios. For HPALD chemistry, we adapted two different

395 HPALD formation rate constants published by Peeters and Muller (2010) and Crounse et

396 al. (2011). The formation rates from Peeters and Muller (2010) is about 40 times faster

397 than those from Crounse et al. (2011) in 298 K. Although there have been speculations

398 about other radical recycling mechanisms such as peroxy radical-peroxy radical reactions

399 (Lelieveld et al., 2008) and unknown reducing agents showing similar chemical

400 behaviors as NO (Hofzumahaus et al., 2009), we do not evaluate these possibilities as

401 there are no specific chemical mechanisms.

402   Modeled OH, HO_2, and RO_2 from the six different model scenarios are shown in

403 Figure 3. A summary of averaged OH, HO_2, and RO_2 concentrations in the morning

404 (08:00 – 11:00) and the afternoon (13:00 – 16:00) from each simulation is shown in

405 Table 4. With respect to the base run results (Scenario I), Scenario III with the lower

406 HPALD formation rate does not cause noticeable differences in radical concentrations.

407 Adapting higher HPALD formation rates (Scenario II) cause significant differences in

408 radical distribution especially in RO_2. This difference is likely caused by the fact that

409 significant isoprene peroxy radical is converted to HPALD. The higher levels of

410 discrepancy is found in RO_2 between Scenario I and Scenario II in the afternoon when

411 low NO concentrations are observed, which efficiently facilitates HPALD formation.

412 Similarly, a larger OH discrepancy (~ 20 %) between Scenario I and Scenario II is

413 observed in the afternoon.

414   Striking differences can be found in the model simulation results with or without

415 constraining observed HONO as shown in Figure 3. Model calculation results from

416 Scenario IV indicate significantly smaller OH, HO_2, and RO_2 concentrations than the

417 concentrations calculated from the counter part (Scenario I), which contains identical

418 constraints and isoprene photochemistry except constraining observed HONO. Again,

419 this clearly indicates that more thorough evaluations of the impacts of HONO on air

420 quality are needed to precisely constrain photochemical processes in the region along

421 with evaluations of the currently available analytical techniques as argued in section 3.1.

422

423 **3.3 Implications of the uncertainty in HO_X estimations in assessing photochemical**

424 **ozone and OVOC production.**

425 Two competing chemical reactions (R3 vs. R4,5,6) determine radical distribution

426 regimes.

427 $$RO_2 + NO \rightarrow RO + NO_2 \text{ (R3)}$$

428 $$RO_2 + HO_2 \rightarrow ROOH + O_2 \text{ (R4)}$$

429 $$RO_2 + RO_2 \rightarrow ROOR + O_2 \text{ (R5)}$$

430 $$HO_2 + HO_2 \rightarrow H_2O_2 + O_2 \text{ (R6)}$$

431

432 When the rate of R3 gets much faster than the sum of reaction rates of R4, R5,

433 and R6 then radical recycling processes become more efficient than radical destruction

434 processes. In this radical recycling regime, OH, a universal tropospheric oxidant, is well

435 buffered to maintain the elevated OH levels. On the other hand, the radical destruction

436 regime can be defined when the radical recycling rates (R3) are slower than the radical

437 destruction reaction rates (R4+R5+R6). Although some recent field studies (e.g.

438 Lelieveld et al. (2008)) suggest that we may need to reconsider R4 as a radical recycling

439 process rather than a radical destruction process, in this study, we follow the conventional

440 classification of radical chemistry regimes since recent laboratory characterizations have

441 shown that OH recycling from the $RO_2 + HO_2$ reaction should be insignificant (Liu et al.,

442   2013;Villena et al., 2012;Fuchs et al., 2013) . The temporal variations of radical-radical

443   reaction rates from the model simulation scenarios are shown in Figure 4. In general, the

444   radical reaction rates are elevated as much as twice once observed HONO is constrained

445   in the model calculations (e.g. Scenario IV). This is because unaccounted HONO in the

446   model calculations cause significant underestimations in the radical pool ($OH+HO_2+RO_2$)

447   size with respect to the constrained HONO scenarios as shown in Figure 4. In addition, as

448   we include recently developed isoprene radical chemistry, the RO_2+HO_2 reaction rates,

449   known for a radical destruction pathway becomes higher. This becomes more obvious in

450   the afternoon when NO concentration becomes lower. Especially, in the case of Scenario

451   II, the $RO_2 + HO_2$ reaction rates get close or slightly higher than those of $RO_2 + NO$ in

452   the afternoon . This is surprising, as the radical destruction regime is usually associated

453   with low NO_X conditions. Suburban regions of megacities including the TRF in general

454   show high NO_X conditions. However, radical recycling rates are determined by

455   concentrations of NO. The fraction of NO in the NO_X pool is determined by competing

456   reactions between NO_2 photolysis and oxidation reactions of NO by ozone, HO_2, and

457   RO_2 radicals. Once we assume the pseudo-steady state of NO, then NO in NO_X pool

458   (Leighton, 1961) can be expressed as

459

460        $[NO] = J_{NO2}[NO_2]/(k_{NO+O3}[O_3] + k_{NO+HO2}[HO_2] + k_{NO+RO2}[RO_2])$ (Eq 1)

461

462   This mathematical expression clearly shows that NO levels are dependent on NO_X

463   mostly composed of NO_2. At the same time, the fraction of NO in NO_X is anti-correlated

464   with ozone, HO_2, and RO_2 concentrations. Therefore, the size of the radical pool

465   composed of HO_2 and RO_2 is relevant for determining the fractions of NO in given NO_X

466   levels. High HO_2 and RO_2 are likely observed in high VOC regions such as forested areas.

467   This could cause a smaller fraction of NO in the given NO_X pool so radical recycling gets

468   relatively weaker compared with radical destruction reaction pathways. More quantitative

469   approaches are required to categorize radical reaction pathways rather than qualitative

470   categorization such as high or low NO_X regimes. One should keep in mind that the

471   pseudo-steady state assumption requires precise NO_2 quantification, which may not be

472   the case in our study as the Mo-converter used for the NO_2 quantification could have

473   interferences (Table 1). The overestimation due to thermal dissociations of reactive

474   oxygenated nitrogen species has been reported to be 20 % to 83 % (Ge et al.,

475   2013;Steinbacher et al., 2007). In addition, Mannschreck et al. (2004) presented the NO-

476   NO_2-ozone photostationary state analysis using a four year dataset from a rural

477   observational site in Hohenpeissenberg, Germany. The results indicate that the pseudo

478   steady state assumption considering only NO-NO_2-ozone deviates about a factor of two

479   from the stationary state on average. Even with the consideration of peroxy radical

480   chemistry the pseudo steady state assumption is only valid for 13-32 % of the

481   observational period. The authors speculated that local NO_2 sources, local NO or ozone

482   sinks, or rapid changes in J_{NO2} and ozone can break the pseudo-steady state. Nonetheless,

483   the argument that NO is a more critical parameter in determining radical distributions

484   than NO_X levels still holds.

485   Conventionally, efficient ozone production can be achieved by the balance

486   between nitric acid production rates (P_{HNO3}, $OH + NO_2$) and peroxide production rates

487   (P_{ROOH}, HO_2+RO_2 or P_{H2O2} HO_2+HO_2) (Sillman and He, 2002). The imbalance will cause

488 ozone production sensitivity towards either NOx or VOCs. A comprehensive

489 photochemical model analysis (Tonnesen and Dennis, 2000a, b) demonstrated that in a

490 wider range of ozone concentrations, the VOC and NOx limited regimes can be

491 determined by the ratios of P_{H2O2} and P_{HNO3}. Kleinman (2000) and Sillman and He (2002)

492 presented an observation-based ozone production regime evaluation method comparing

493 peroxide production rates (P(peroxide)) and nitric acid production rates ($P(HNO_3)$). This

494 categorization has guided policy-making processes whether NO_X or VOC controls will be

495 more effective in ozone reduction. A series of modeling studies have been conducted to

496 characterize ozone production regimes in the suburban regions of East Asian megacities

497 and have consistently concluded that the role of isoprene is important in ozone

498 production. However, most of these studies have concluded that East Asian megacity

499 regions are mostly in the VOC limited regime (Tseng et al., 2009;Zhang et al.,

500 2008b;Lim et al., 2011;Cheng et al., 2010;Shao et al., 2009a;Shao et al., 2009b;Xing et

501 al., 2011). Recently, however, a modeling study by Li et al. (2013) in the Pearl River

502 Delta region in China demonstrated the time dependence of ozone production regimes.

503 Specifically, with high NOx emissions in the morning, the regional ozone production

504 regime is categorized as VOC limited. In contrast, in the afternoon when the highest

505 ozone concentrations are observed, a NOx limited regime is often found. The obvious

506 issue to be addressed is that all of the above studies neglected how the uncertainty in

507 hydroxyl radical chemistry would affect the ozone production regime. Moreover, HONO

508 has been rarely constrained by observations in the previous modeling studies. Figure 5

509 shows the temporal variations of 2 P(peroxide)/$P(HNO_3)$ from all four different model

510 scenarios. As shown in the figure, the ratio above 1 indicates the NO_X limited regime and

511   the VOC limited regime can be determined when the ratio is below 1. The NO_X limited

512   ozone formation regime occurred on most days except the morning when high NO_X

513   levels were observed regardless of the HO_X simulation scenarios. This is consistent with

514   the recent modeling study for the Pearl River Delta region by Li et al. (2013). Differences

515   among the scenarios are not noticeable in the morning when NO is high but noticeable

516   differences can be found in the afternoon which may cause uncertainty in assessing the

517   optimal level of NO_X and VOC emission controls from a policy perspective. In general,

518   the model calculation results with faster HPALD formation rates indicate lower

519   P(peroxide)/P(HNO_3) in the afternoon. This analysis indicates that it is difficult to

520   determine an effective policy implementation for NO_X or VOC controls to achieve ozone

521   abatement around Asian megaticities where isoprene is a significant OH sink without

522   accurate understanding of radical-isoprene interactions (e.g. Kim et al. (2013b)).

523   Another unresolved uncertainty in understanding tropospheric OH is its chemical

524   loss rates. The limited observations of OH reactivity in BVOC dominant environments

525   show consistent unaccounted OH chemical loss with observational datasets (Di Carlo et

526   al., 2004;Edwards et al., 2013;Kim et al., 2011;Lou et al., 2010;Nolscher et al.,

527   2012;Nakashima et al., 2014;Sinha et al., 2010). Two different processes are speculated

528   to cause unaccounted OH loss known as missing OH reactivity: 1) primary emissions of

529   unmeasured or unknown compounds and 2) oxidation products of well-known BVOCs

530   especially isoprene. Most studies conducted in coniferous forests where monoterpenes

531   are dominant primary BVOC emissions have concluded that unmeasured or unknown

532   primary BVOC emissions caused missing OH reactivity (Sinha et al., 2010;Nakashima et

533   al., 2014). On the other hand, studies conducted in isoprene dominant environments in

534 mostly broadleaf or mixed forests have concluded that the main cause of missing OH

535 reactivity is the oxidation products of isoprene (Edwards et al., 2013;Kim et al., 2011).

536 Edwards et al. (2013) presented a thorough analysis on potential impacts of isoprene

537 oxidation products that are not routinely constrained by observations. The authors found

538 significant contributions from secondary oxidation products such as multi-functional

539 oxygenated compounds.

540   Figure 6a shows the temporal variations of total OH reactivity calculated from

541 five different model scenarios (I through IV). The highest and the lowest OH reactivity

542 levels were predicted from model calculations of Scenario I and Scenario IV, respectively.

543 This observation is directly correlated with calculated RO_2 levels as the lowest and

544 highest RO_2 levels were calculated from Scenario I and Scenario IV, respectively. Since

545 VOC precursors and trace gases were all constrained by observations in the model

546 calculations, the differences in model calculated OH reactivity should be mainly caused

547 by the oxidation products of VOCs. This can be confirmed by the comparisons of model

548 calculated formaldehyde concentrations from Scenario I and IV as formaldehyde is a

549 dominant oxidation product of isoprene (Figure 6b). The differences in formaldehyde

550 levels suggest differences in OH reactivity levels from OVOCs in each model simulation.

551 In summary, uncertainty in radical distributions especially RO_2 levels is directly

552 propagated into uncertainty in OVOC formation.

553   These calculated results provide an upper limit of potential contributions from the

554 oxidation products of the constrained VOC precursors considering that the box-model

555 does not consider dry-deposition processes as Karl et al. (2010) and Edwards et al. (2013)

556 suggested that there is significant uncertainty associated with the parameterizations of dry

557 deposition especially OVOCs. Still, this analysis suggests that significant missing OH

558 reactivity (~ up to factor of two to three) can be found without constraining OVOCs.

559 OVOCs, especially multi-functional highly oxidized compounds are precursors for

560 secondary organic aerosols (VOCs). Therefore, uncertainty surrounding missing OH

561 reactivity significantly undermines our ability to constrain SOA formation and aerosol

562 growth.

563

564 **4. Summary and conclusions**

565   We presented trace gas observation results from the TRF near the center of Seoul,

566 South Korea. The dataset provides important constraints to evaluate the HO_X pool at the

567 site where both anthropogenic and biogenic influences become important factors in

568 determining oxidation capacity. Although the site is in the vicinity of a megacity with 25

569 million people, isoprene accounted for most of the OH loss from observed atmospheric

570 hydrocarbon species during the 6-day focus period in early June 2012 during a regional

571 pollution episode. In addition, observed NO_X levels were substantially lower than

572 observed values in the center of the SMA. These observations indicate that impacts of

573 megacity pollution on suburban BVOC photochemistry can be observed at the TRF.

574   Four different model scenarios are employed to investigate the radical (OH, HO_2,

575 and RO_2) distributions using the UWCM box-model. The observed trace gas data were

576 constrained and the photochemical mechanisms (MCM 3.2) of seven VOC species with

577 high levels at the TRF were integrated. The uncertainty in isoprene peroxy radical

578 chemistry results in a wider range of OH, HO_2, and RO_2 distributions. Unconstrained

579 HONO sources also cause a quite high level of underestimation in a radical pool

580 (OH+HO$_2$+RO$_2$). OH simulation from the different model scenarios indicates much

581 larger discrepancies (up to three times) than simulations for HO$_2$ and RO$_2$ (up to twofold).

582 OH is simulated in higher levels with the consideration of an additional OH recycling

583 channel from fast HPALD formation chemistry Peeters and Muller (2010). On the other

584 hand, the RO$_2$ simulations result in lower levels as HPALD formation depletes the RO$_2$

585 pool, which mostly composed by isoprene peroxy radicals. These results suggest that

586 direct HO$_2$ and RO$_2$ observations can provide pivotal information about radical recycling

587 and isoprene peroxy radical chemistry (Kim et al., 2013c;Wolfe et al., 2013). More

588 studies on characterizing existing techniques to quantify HO$_2$ (Fuchs et al., 2011) and

589 developing new techniques (Horstjann et al., 2013) are needed. In addition, the

590 simulations with recently developed isoprene photo-oxidation chemistry show that

591 radical termination processes (e.g. peroxide formation) get more efficient than radical

592 recycling processes in the afternoon. This may come as a surprise as in general we expect

593 the high NO$_X$ conditions in the suburban regions of a megacity to have effective radical

594 recycling. However, the critical factor determining competing reaction channels of

595 recycling and peroxide formation is NO concentrations. Ratios of NO to NO$_2$ are not only

596 correlated with NO$_2$ concentrations and photolysis constants but also anti-correlated with

597 RO$_2$, HO$_2$ and ozone concentrations and relevant kinetic constants as shown in (Eq 1).

598 Therefore, a semi-quantitative term such as the high 'NO$_X$' regime is not a proper term to

599 define radical recycle regimes especially in high radical environments (e.g. HO$_2$ and RO$_2$)

600 such as forest environments.

601   These uncertainties in estimating the radical pool size and distribution directly

602 affect our ability for constraining photochemical ozone and OVOC production. The non-

603   linear response of ozone production to NO_X and VOC abundances are determined by OH,

604   HO_2, RO_2 and NO_2 concentrations. Regardless of which model calculation scenario we

605   adapt, the TRF photochemical state appears to be a NO_X limited ozone production regime,

606   except for the morning when the VOC limited regime is observed. A noticeable range of

607   NO_X sensitivity was calculated from the four different model scenarios, especially in the

608   afternoon. These analysis results, therefore, suggest that an accurate scientific

609   understanding of isoprene-OH interactions should form the basis for an effective policy

610   implementation to reduce photochemical pollution in the suburbs of Seoul and similar

611   East Asian megacities. In addition, OVOC production is predicted to significantly vary

612   depending on the model simulation scenarios. The fate of these OVOCs is uncertain and

613   can include deposition, photolysis, or condensation. Our limited understanding of

614   OVOCs contributes substantially to the overall uncertainty in radical photochemistry and

615   should be addressed by studies that quantify the processes controlling OVOC production

616   and loss.

617

622
623   **References**
624

625   Apel, E. C., Riemer, D. D., Hills, A., Baugh, W., Orlando, J., Faloona, I., Tan, D., Brune,
626   W., Lamb, B., Westberg, H., Carroll, M. A., Thornberry, T., and Geron, C. D.:
627   Measurement and interpretation of isoprene fluxes and isoprene, methacrolein, and

628   methyl vinyl ketone mixing ratios at the PROPHET site during the 1998 Intensive,
629   J Geophys Res-Atmos, 107, Artn 4034

630   Doi 10.1029/2000jd000225, 2002.

631   Archibald, A. T., Cooke, M. C., Utembe, S. R., Shallcross, D. E., Derwent, R. G., and
632   Jenkin, M. E.: Impacts of mechanistic changes on HOx formation and recycling in
633   the oxidation of isoprene, Atmos Chem Phys, 10, 8097-8118, Doi 10.5194/Acp-
634   10-8097-2010, 2010a.

635   Archibald, A. T., Jenkin, M. E., and Shallcross, D. E.: An isoprene mechanism
636   intercomparison, Atmos Environ, 44, 5356-5364, Doi
637   10.1016/J.Atmosenv.2009.09.016, 2010b.

638   Arneth, A., Schurgers, G., Lathiere, J., Duhl, T., Beerling, D. J., Hewitt, C. N., Martin,
639   M., and Guenther, A.: Global terrestrial isoprene emission models: sensitivity to
640   variability in climate and vegetation, Atmos Chem Phys, 11, 8037-8052, Doi
641   10.5194/Acp-11-8037-2011, 2011.

642   Bao, H., Shrestha, K. L., Kondo, A., Kaga, A., and Inoue, Y.: Modeling the influence of
643   biogenic volatile organic compound emissions on ozone concentration during
644   summer season in the Kinki region of Japan, Atmos Environ, 44, 421-431, Doi
645   10.1016/J.Atmosenv.2009.10.021, 2010.

646   Barket, D. J., Hurst, J. M., Couch, T. L., Colorado, A., Shepson, P. B., Riemer, D. D.,
647   Hills, A. J., Apel, E. C., Hafer, R., Lamb, B. K., Westberg, H. H., Farmer, C. T.,
648   Stabenau, E. R., and Zika, R. G.: Intercomparison of automated methodologies for
649   determination of ambient isoprene during the PROPHET 1998 summer campaign,
650   J Geophys Res-Atmos, 106, 24301-24313, Doi 10.1029/2000jd900562, 2001.

651   Blake, R. S., Monks, P. S., and Ellis, A. M.: Proton-Transfer Reaction Mass
652   Spectrometry, Chem Rev, 109, 861-896, 2009.

653   Bryan, A. M., Bertman, S. B., Carroll, M. A., Dusanter, S., Edwards, G. D., Forkel, R.,
654   Griffith, S., Guenther, A. B., Hansen, R. F., Helmig, D., Jobson, B. T., Keutsch, F.
655   N., Lefer, B. L., Pressley, S. N., Shepson, P. B., Stevens, P. S., and Steiner, A. L.:
656   In-canopy gas-phase chemistry during CABINEX 2009: sensitivity of a 1-D
657   canopy model to vertical mixing and isoprene chemistry, Atmos Chem Phys, 12,
658   8829-8849, Doi 10.5194/Acp-12-8829-2012, 2012.

659   Chameides, W. L., Lindsay, R. W., Richardson, J., and Kiang, C. S.: The Role of
660   Biogenic Hydrocarbons in Urban Photochemical Smog - Atlanta as a Case-Study,
661   Science, 241, 1473-1475, 1988.

662   Chang, C. C., Wang, J. L., Leung, S.-C. C., Chang, C. Y., Lee, P.-J., Chew, C., Liao, W.-
663   N., and Ou-Yang, C.-F.: Seosonal characteristics of biogenic and anthropogenic

664   isoprene in tropical-subtropical urban environments, Atmos Environ, 99, 298-308,
665   2014.

666   Cheng, H. R., Guo, H., Saunders, S. M., Lam, S. H. M., Jiang, F., Wang, X. M., Simpson,
667   I. J., Blake, D. R., Louie, P. K. K., and Wang, T. J.: Assessing photochemical
668   ozone formation in the Pearl River Delta with a photochemical trajectory model,
669   Atmos Environ, 44, 4199-4208, Doi 10.1016/J.Atmosenv.2010.07.019, 2010.

670   Crounse, J. D., Paulot, F., Kjaergaard, H. G., and Wennberg, P. O.: Peroxy radical
671   isomerization in the oxidation of isoprene, Phys Chem Chem Phys, 13, 13607-
672   13613, Doi 10.1039/C1cp21330j, 2011.

673   de Gouw, J., and Warneke, C.: Measurements of volatile organic compounds in the
674   Earth's atmosphere using proton-transfer-reaction mass spectrometry, Mass
675   Spectrom Rev, 26, 223-257, 2007.

676   Di Carlo, P., Brune, W. H., Martinez, M., Harder, H., Lesher, R., Ren, X. R., Thornberry,
677   T., Carroll, M. A., Young, V., Shepson, P. B., Riemer, D., Apel, E., and Campbell,
678   C.: Missing OH reactivity in a forest: Evidence for unknown reactive biogenic
679   VOCs, Science, 304, 722-725, Doi 10.1126/Science.1094392, 2004.

680   Dreyfus, G. B., Schade, G. W., and Goldstein, A. H.: Observational constraints on the
681   contribution of isoprene oxidation to ozone production on the western slope of the
682   Sierra Nevada, California, J Geophys Res-Atmos, 107, Artn 4365 Doi
683   10.1029/2001jd001490, 2002.

684   Edwards, P. M., Evans, M. J., Furneaux, K. L., Hopkins, J., Ingham, T., Jones, C., Lee, J.
685   D., Lewis, A. C., Moller, S. J., Stone, D., Whalley, L. K., and Heard, D. E.: OH
686   reactivity in a South East Asian tropical rainforest during the Oxidant and Particle
687   Photochemical Processes (OP3) project, Atmos Chem Phys, 13, 9497-9514, Doi
688   10.5194/Acp-13-9497-2013, 2013.

689   Fuchs, H., Bohn, B., Hofzumahaus, A., Holland, F., Lu, K. D., Nehr, S., Rohrer, F., and
690   Wahner, A.: Detection of HO_2 by laser-induced fluorescence: calibration and
691   interferences from RO2 radicals, Atmos Meas Tech, 4, 1209-1225, Doi
692   10.5194/Amt-4-1209-2011, 2011.

693   Fuchs, H., Hofzumahaus, A., Rohrer, F., Bohn, B., Brauers, T., Dorn, H. P., Haseler, R.,
694   Holland, F., Kaminski, M., Li, X., Lu, K., Nehr, S., Tillmann, R., Wegener, R., and
695   Wahner, A.: Experimental evidence for efficient hydroxyl radical regeneration in
696   isoprene oxidation, Nat Geosci, 6, 1023-1026, Doi 10.1038/Ngeo1964, 2013.

697   Ge, B. Z., Sun, Y. L., Liu, Y., Dong, H. B., Ji, D. S., Jiang, Q., Li, J., and Wang, Z. F.:
698   Nitrogen dioxide measurement by cavity attenuated phase shift spectroscopy
699   (CAPS) and implications in ozone production efficiency and nitrate formation in

700   Beijing, China, J Geophys Res-Atmos, 118, 9499-9509, Doi 10.1002/Jgrd.50757,
701   2013.

702 Guenther, A.: Biological and chemical diversity of biogenic volatile organic emissions
703   into the atmosphere, Atmospheric Sciences, 2013, ArticleID 786290, 2013.

704 Hao, N., Zhou, B., Chen, D., and Chen, L. M.: Observations of nitrous acid and its
705   relative humidity dependence in Shanghai, J Environ Sci-China, 18, 910-915, Doi
706   10.1016/S1001-0742(06)60013-2, 2006.

707 Hofzumahaus, A., Rohrer, F., Lu, K. D., Bohn, B., Brauers, T., Chang, C. C., Fuchs, H.,
708   Holland, F., Kita, K., Kondo, Y., Li, X., Lou, S. R., Shao, M., Zeng, L. M.,
709   Wahner, A., and Zhang, Y. H.: Amplified Trace Gas Removal in the Troposphere,
710   Science, 324, 1702-1704, 10.1126/science.1164566, 2009.

711 Horstjann, M., Andres Hernandez, M. D., Nenakhov, V., Chrobry, A., and Burrows, J. P.:
712   Peroxy radical detection for airborne atmospheric measurements using cavity
713   ehnaced absorption spectroscopy of NO_2, Atmospheric Measurement Techniques
714   Discussion, 6, 9655-9688, 2013.

715 Huang, M., Bowman, K. W., Carmichael, G. R., Pierce, R. B., Worden, H. M., Luo, M.,
716   Cooper, O. R., Pollack, I. B., Ryerson, T. B., and Brown, S. S.: Impact of Southern
717   California anthropogenic emissions on ozone pollution in the mountain states:
718   Model analysis and observational evidence from space, J Geophys Res-Atmos,
719   118, 12784-12803, Doi 10.1002/2013jd020205, 2013.

720 Karl, T., Harley, P., Emmons, L., Thornton, B., Guenther, A., Basu, C., Turnipseed, A.,
721   and Jardine, K.: Efficient Atmospheric Cleansing of Oxidized Organic Trace
722   Gases by Vegetation, Science, 330, 816-819, Doi 10.1126/Science.1192534, 2010.

723 Kim, K. H., Ho, D. X., Park, C. G., Ma, C. J., Pandey, S. K., Lee, S. C., Jeong, H. J., and
724   Lee, S. H.: Volatile Organic Compounds in Ambient Air at Four Residential
725   Locations in Seoul, Korea, Environ Eng Sci, 29, 875-889, Doi
726   10.1089/Ees.2011.0280, 2012.

727 Kim, S., Karl, T., Guenther, A., Tyndall, G., Orlando, J., Harley, P., Rasmussen, R., and
728   Apel, E.: Emissions and ambient distributions of Biogenic Volatile Organic
729   Compounds (BVOC) in a ponderosa pine ecosystem: interpretation of PTR-MS
730   mass spectra, Atmos Chem Phys, 10, 1759-1771, 2010.

731 Kim, S., Guenther, A., Karl, T., and Greenberg, J.: Contributions of primary and
732   secondary biogenic VOC tototal OH reactivity during the CABINEX (Community
733   Atmosphere-Biosphere INteractions Experiments)-09 field campaign, Atmos
734   Chem Phys, 11, 8613-8623, 2011.

735 Kim, S., Guenther, A., and Apel, E.: Quantitative and qualitative sensing techniques for
736   biogenic volatile organic compounds and their oxidation products, Environ Sci-
737   Proc Imp, 15, 1301-1314, Doi 10.1039/C3em00040k, 2013a.

738 Kim, S., Lee, M., Kim, S., Choi, S., Seok, S., and Kim, S.: Photochemical characteristics
739   of high and low ozone episodes observed in the Taehwa Forest observatory (TFO)
740   in June 2011 near Seoul South Korea, Asia-Pacific Journal of Atmospheric
741   Sciences, 49, 325-331, Doi 10.1007/S13143-013-0031-0, 2013b.

742 Kim, S., Wolfe, G. M., Mauldin, L., Cantrell, C., Guenther, A., Karl, T., Turnipseed, A.,
743   Greenberg, J., Hall, S. R., Ullmann, K., Apel, E., Hornbrook, R., Kajii, Y.,
744   Nakashima, Y., Keutsch, F. N., DiGangi, J. P., Henry, S. B., Kaser, L.,
745   Schnitzhofer, R., Graus, M., Hansel, A., Zheng, W., and Flocke, F. F.: Evaluation
746   of HOx sources and cycling using measurement-constrained model calculations in
747   a 2-methyl-3-butene-2-ol (MBO) and monoterpene (MT) dominated ecosystem,
748   Atmos Chem Phys, 13, 2031-2044, Doi 10.5194/Acp-13-2031-2013, 2013c.

749 Kim, S., VandenBoer, T. C., Young, C. J., Riedel, T. P., Thornton, J. A., Swarthout, B.,
750   Sive, B., Lerner, B., Gilman, J. B., Warneke, C., Roberts, J. M., Guenther, A.,
751   Wagner, N. L., Dube, W. P., Williams, E., and Brown, S. S.: The primary and
752   recycling sources of OH during the NACHTT-2011 campaign: HONO as an
753   important OH primary source in the wintertime, J Geophys Res-Atmos, 119, 6886-
754   6896, Doi 10.1002/2013jd019784, 2014.

755 Kim, S. Y., Jiang, X. Y., Lee, M., Turnipseed, A., Guenther, A., Kim, J. C., Lee, S. J.,
756   and Kim, S.: Impact of biogenic volatile organic compounds on ozone production
757   at the Taehwa Research Forest near Seoul, South Korea, Atmos Environ, 70, 447-
758   453, Doi 10.1016/J.Atmosenv.2012.11.005, 2013d.

759 Kleinman, L. I.: Ozone process insights from field experiments - part II: Observation-
760   based analysis for ozone production, Atmos Environ, 34, 2023-2033, Doi
761   10.1016/S1352-2310(99)00457-4, 2000.

762 Leighton, P. A.: Photochemistry of Air Pollution, Academic, San Diego, CA USA, 1961.

763 Lelieveld, J., Butler, T. M., Crowley, J. N., Dillon, T. J., Fischer, H., Ganzeveld, L.,
764   Harder, H., Lawrence, M. G., Martinez, M., Taraborrelli, D., and Williams, J.:
765   Atmospheric oxidation capacity sustained by a tropical forest, Nature, 452, 737-
766   740, 2008.

767 Levy, H.: Normal Atmosphere - Large Radical and Formaldehyde Concentrations
768   Predicted, Science, 173, 141-143, 1971.

769 Li, X., Brauers, T., Haseler, R., Bohn, B., Fuchs, H., Hofzumahaus, A., Holland, F., Lou,
770   S., Lu, K. D., Rohrer, F., Hu, M., Zeng, L. M., Zhang, Y. H., Garland, R. M., Su,
771   H., Nowak, A., Wiedensohler, A., Takegawa, N., Shao, M., and Wahner, A.:

772   Exploring the atmospheric chemistry of nitrous acid (HONO) at a rural site in
773   Southern China, Atmos Chem Phys, 12, 1497-1513, Doi 10.5194/Acp-12-1497-
774   2012, 2012.

775 Li, Y., Lau, A. K. H., Fung, J. C. H., Zheng, J. Y., and Liu, S. C.: Importance of NOx
776   control for peak ozone reduction in the Pearl River Delta region, J Geophys Res-
777   Atmos, 118, 9428-9443, Doi 10.1002/Jgrd.50659, 2013.

778 Lim, Y. J., Armendariz, A., Son, Y. S., and Kim, J. C.: Seasonal variations of isoprene
779   emissions from five oak tree species in East Asia, Atmos Environ, 45, 2202-2210,
780   Doi 10.1016/J.Atmosenv.2011.01.066, 2011.

781 Liu, Y. J., Herdlinger-Blatt, I., McKinney, K. A., and Martin, S. T.: Production of methyl
782   vinyl ketone and methacrolein via the hydroperoxyl pathway of isoprene oxidation,
783   Atmospheric Chemistry and Physics, 13, 5715-5730, Doi 10.5194/Acp-13-5715-
784   2013, 2013.

785 Lou, S., Holland, F., Rohrer, F., Lu, K., Bohn, B., Brauers, T., Chang, C. C., Fuchs, H.,
786   Haseler, R., Kita, K., Kondo, Y., Li, X., Shao, M., Zeng, L., Wahner, A., Zhang,
787   Y., Wang, W., and Hofzumahaus, A.: Atmospheric OH reactivities in the Pearl
788   River Delta - China in summer 2006: measurement and model results, Atmos
789   Chem Phys, 10, 11243-11260, Doi 10.5194/Acp-10-11243-2010, 2010.

790 Lu, K. D., Rohrer, F., Holland, F., Fuchs, H., Bohn, B., Brauers, T., Chang, C. C.,
791   Haseler, R., Hu, M., Kita, K., Kondo, Y., Li, X., Lou, S. R., Nehr, S., Shao, M.,
792   Zeng, L. M., Wahner, A., Zhang, Y. H., and Hofzumahaus, A.: Observation and
793   modelling of OH and HO2 concentrations in the Pearl River Delta 2006: a missing
794   OH source in a VOC rich atmosphere, Atmos Chem Phys, 12, 1541-1569, Doi
795   10.5194/Acp-12-1541-2012, 2012.

796 Ma, J. Z., Wang, W., Chen, Y., Liu, H. J., Yan, P., Ding, G. A., Wang, M. L., Sun, J., and
797   Lelieveld, J.: The IPAC-NC field campaign: a pollution and oxidization pool in the
798   lower atmosphere over Huabei, China, Atmos Chem Phys, 12, 3883-3908, Doi
799   10.5194/Acp-12-3883-2012, 2012.

800 Mannschreck, K., Gilge, S., Plass-Duelmer, C., Fricke, W., and Berresheim, H.:
801   Assessment of the applicability of NO-NO2-O-3 photostationary state to long-term
802   measurements at the Hohenpeissenberg GAW Station, Germany, Atmos Chem
803   Phys, 4, 1265-1277, 2004.

804 Mao, J., Ren, X., Zhang, L., Van Duin, D. M., Cohen, R. C., Park, J. H., Goldstein, A. H.,
805   Paulot, F., Beaver, M. R., Crounse, J. D., Wennberg, P. O., DiGangi, J. P., Henry,
806   S. B., Keutsch, F. N., Park, C., Schade, G. W., Wolfe, G. M., Thornton, J. A., and
807   Brune, W. H.: Insights into hydroxyl measurements and atmospheric oxidation in a
808   California forest, Atmos Chem Phys, 12, 8009-8020, Doi 10.5194/Acp-12-8009-
809   2012, 2012.

810 Mao, J. Q., Ren, X. R., Chen, S. A., Brune, W. H., Chen, Z., Martinez, M., Harder, H.,
811   Lefer, B., Rappengluck, B., Flynn, J., and Leuchner, M.: Atmospheric oxidation
812   capacity in the summer of Houston 2006: Comparison with summer measurements
813   in other metropolitan studies, Atmos Environ, 44, 4107-4115, Doi
814   10.1016/J.Atmosenv.2009.01.013, 2010.

815 Na, K., and Kim, Y. P.: Seasonal characteristics of ambient volatile organic compounds
816   in Seoul, Korea, Atmos Environ, 35, 2603-2614, Doi 10.1016/S1352-
817   2310(00)00464-7, 2001.

818 Nakashima, Y., Kato, S., Greenberg, J., Harley, P., Karl, T., Turnipseed, A., Apel, E.,
819   Guenther, A., Smith, J., and Kajii, Y.: Total OH reactivity measurements in
820   ambient air in a southern Rocky mountain ponderosa pine forest during
821   BEACHON-SRM08 summer campaign, Atmos Environ, 85, 1-8, Doi
822   10.1016/J.Atmosenv.2013.11.042, 2014.

823 NIER: Annual Report for Atmospheric Environment, National Insititute of Environmetal
824   Rsearch, 2010.

825 Nolscher, A. C., Williams, J., Sinha, V., Custer, T., Song, W., Johnson, A. M., Axinte,
826   R., Bozem, H., Fischer, H., Pouvesle, N., Phillips, G., Crowley, J. N., Rantala, P.,
827   Rinne, J., Kulmala, M., Gonzales, D., Valverde-Canossa, J., Vogel, A., Hoffmann,
828   T., Ouwersloot, H. G., de Arellano, J. V. G., and Lelieveld, J.: Summertime total
829   OH reactivity measurements from boreal forest during HUMPPA-COPEC 2010,
830   Atmos Chem Phys, 12, 8257-8270, Doi 10.5194/Acp-12-8257-2012, 2012.

831 Oswald, R., Behrendt, T., Ermel, M., Wu, D., Su, H., Cheng, Y., Breuninger, C.,
832   Moravek, A., Mougin, E., Delon, C., Loubet, B., Pommerening-Roser, A., Sorgel,
833   M., Poschl, U., Hoffmann, T., Andreae, M. O., Meixner, F. X., and Trebs, I.:
834   HONO Emissions from Soil Bacteria as a Major Source of Atmospheric Reactive
835   Nitrogen, Science, 341, 1233-1235, Doi 10.1126/Science.1242266, 2013.

836 Paulot, F., Crounse, J. D., Kjaergaard, H. G., Kroll, J. H., Seinfeld, J. H., and Wennberg,
837   P. O.: Isoprene photooxidation: new insights into the production of acids and
838   organic nitrates, Atmos Chem Phys, 9, 1479-1501, 2009.

839 Paulson, S. E., and Seinfeld, J. H.: Development and evaluation of a photooxidation
840   mechanism for isoprene, Journal of Geophysical Research, 97, 20703-20715,
841   1992.

842 Peeters, J., and Muller, J. F.: HOx radical regeneration in isoprene oxidation via peroxy
843   radical isomerisations. II: experimental evidence and global impact, Phys Chem
844   Chem Phys, 12, 14227-14235, Doi 10.1039/C0cp00811g, 2010.

845 Pollack, I. B., Ryerson, T. B., Trainer, M., Neuman, J. A., Roberts, J. M., and Parrish, D.
846   D.: Trends in ozone, its precursors, and related secondary oxidation products in

847   Los Angeles, California: A synthesis of measurements from 1960 to 2010, J
848   Geophys Res-Atmos, 118, 5893-5911, Doi 10.1002/Jgrd.50472, 2013.

849 Ran, L., Zhao, C. S., Xu, W. Y., Lu, X. Q., Han, M., Lin, W. L., Yan, P., Xu, X. B.,
850   Deng, Z. Z., Ma, N., Liu, P. F., Yu, J., Liang, W. D., and Chen, L. L.: VOC
851   reactivity and its effect on ozone production during the HaChi summer campaign,
852   Atmos Chem Phys, 11, 4657-4667, Doi 10.5194/Acp-11-4657-2011, 2011.

853 Ren, X., Sanders, J. E., Rajendran, A., Weber, R. J., Goldstein, A. H., Pusede, S. E.,
854   Browne, E. C., Min, K. E., and Cohen, R. C.: A relaxed eddy accumulation system
855   for measuring vertical fluxes of nitrous acid, Atmos Meas Tech, 4, 2093-2103, Doi
856   10.5194/Amt-4-2093-2011, 2011.

857 Ryerson, T. B., Andrews, A. E., Angevine, W. M., Bates, T. S., Brock, C. A., Cairns, B.,
858   Cohen, R. C., Cooper, O. R., de Gouw, J. A., Fehsenfeld, F. C., Ferrare, R. A.,
859   Fischer, M. L., Flagan, R. C., Goldstein, A. H., Hair, J. W., Hardesty, R. M.,
860   Hostetler, C. A., Jimenez, J. L., Langford, A. O., McCauley, E., McKeen, S. A.,
861   Molina, L. T., Nenes, A., Oltmans, S. J., Parrish, D. D., Pederson, J. R., Pierce, R.
862   B., Prather, K., Quinn, P. K., Seinfeld, J. H., Senff, C. J., Sorooshian, A., Stutz, J.,
863   Surratt, J. D., Trainer, M., Volkamer, R., Williams, E. J., and Wofsy, S. C.: The
864   2010 California Research at the Nexus of Air Quality and Climate Change
865   (CalNex) field study, J Geophys Res-Atmos, 118, 5830-5866, Doi
866   10.1002/Jgrd.50331, 2013.

867 Ryu, Y. H., Baik, J. J., Kwak, K. H., Kim, S., and Moon, N.: Impacts of urban land-
868   surface forcing on ozone air quality in the Seoul metropolitan area, Atmos Chem
869   Phys, 13, 2177-2194, Doi 10.5194/Acp-13-2177-2013, 2013.

870 Sartelet, K. N., Couvidat, F., Seigneur, C., and Roustan, Y.: Impact of biogenic emissions
871   on air quality over Europe and North America, Atmos Environ, 53, 131-141, Doi
872   10.1016/J.Atmosenv.2011.10.046, 2012.

873 Shao, M., Lu, S. H., Liu, Y., Xie, X., Chang, C. C., Huang, S., and Chen, Z. M.: Volatile
874   organic compounds measured in summer in Beijing and their role in ground-level
875   ozone formation, J Geophys Res-Atmos, 114, Artn D00g06 Doi
876   10.1029/2008jd010863, 2009a.

877 Shao, M., Zhang, Y. H., Zeng, L. M., Tang, X. Y., Zhang, J., Zhong, L. J., and Wang, B.
878   G.: Ground-level ozone in the Pearl River Delta and the roles of VOC and NOx in
879   its production, J Environ Manage, 90, 512-518, Doi
880   10.1016/J.Jenvman.2007.12.008, 2009b.

881 Sillman, S., and He, D.: Some theoretical results concerning O_3-NOx-VOC chemistry and
882   NOx-VOC indicators, Journal of Geophysical Research, 107,
883   4659,doi:4610.1029:2001JD001123, 2002.

884 Sinha, V., Williams, J., Lelieveld, J., Ruuskanen, T. M., Kajos, M. K., Patokoski, J.,
885   Hellen, H., Hakola, H., Mogensen, D., Boy, M., Rinne, J., and Kulmala, M.: OH
886   Reactivity Measurements within a Boreal Forest: Evidence for Unknown Reactive
887   Emissions, Environ Sci Technol, 44, 6614-6620, Doi 10.1021/Es101780b, 2010.

888 Song, C. H., Park, M. E., Lee, E. J., Lee, J. H., Lee, B. K., Lee, D. S., Kim, J., Han, J. S.,
889   Moon, K. J., and Kondo, Y.: Possible particulate nitrite formation and its
890   atmospheric implications inferred from the observations in Seoul, Korea, Atmos
891   Environ, 43, 2168-2173, Doi 10.1016/J.Atmosenv.2009.01.018, 2009.

892 Spaulding, R. S., Schade, G. W., Goldstein, A. H., and Charles, M. J.: Characterization of
893   secondary atmospheric photooxidation products: Evidence for biogenic and
894   anthropogenic sources, J Geophys Res-Atmos, 108, Artn 4247 Doi
895   10.1029/2002jd002478, 2003.

896 Steinbacher, M., Zellweger, C., Schwarzenbach, B., Bugmann, S., Buchmann, B.,
897   Ordonez, C., Prevot, A. S. H., and Hueglin, C.: Nitrogen oxide measurements at
898   rural sites in Switzerland: Bias of conventional measurement techniques, J
899   Geophys Res-Atmos, 112, Artn D11307 Doi 10.1029/2006jd007971, 2007.

900 Tie, X., Geng, F., Guenther, A., Cao, J., Greenberg, J., Zhang, R., Apel, E., Li, G.,
901   Weinheimer, A., Chen, J., and Cai, C.: Megacity impacts on regional ozone
902   formation: observations and WRF-Chem modeling for the MIRAGE-Shanghai
903   field campaign, Atmos Chem Phys, 13, 5655-5669, Doi 10.5194/Acp-13-5655-
904   2013, 2013.

905 Tonnesen, G. S., and Dennis, R. L.: Analysis of radical propagation efficiency to assess
906   ozone sensitivity to hydrocarbons and NOx 1. Local indicators of instantaneous
907   odd oxygen production sensitivity, J Geophys Res-Atmos, 105, 9213-9225, Doi
908   10.1029/1999jd900371, 2000a.

909 Tonnesen, G. S., and Dennis, R. L.: Analysis of radical propagation efficiency to assess
910   ozone sensitivity to hydrocarbons and NOx 2. Long-lived species as indicators of
911   ozone concentration sensitivity, J Geophys Res-Atmos, 105, 9227-9241, Doi
912   10.1029/1999jd900372, 2000b.

913 Trainer, M., Williams, E., Parrish, D. D., Buhr, M. P., Allwine, E. J., Westberg, H.,
914   Fehsenfeld, F. C., and Liu, S. C.: Models and observations of the impact of natural
915   hydrocarbons on rural ozone, Nature, 329, 705 - 707, 1987.

916 Tseng, K. H., Wang, J. L., Cheng, M. T., and Tsuang, B. J.: Assessing the Relationship
917   between Air Mass Age and Summer Ozone Episodes Based on Photochemical
918   Indices, Aerosol Air Qual Res, 9, 149-171, 2009.

919 VandenBoer, T., Murphy, J. G., Roberts, J. M., Middlebrook, A. M., Brock, C., Lerner,
920   B. M., Wolfe, D. E., Williams, E., Brown, S. S., Warneke, C., De Gouw, J.,

921   Wagner, N. L., Young, C. C., Dube, W. P., Bahreini, R., Riedel, T., Thornton, J.
922   A., Ozturk, F., Keene, W., Maben, J. R., Pszenny, A., Kim, S., Grossberg, N., and
923   Lefer, B.: Understanding the role of the ground surface in HONO vertical
924   structure: High resolution vertical profiles during NACHTT-11, submitted, 2013.

925   Villena, G., Bejan, I., Kurtenbach, R., Wiesen, P., and Kleffmann, J.: Interferences of
926   commercial NO2 instruments in the urban atmosphere and in a smog chamber,
927   Atmos Meas Tech, 5, 149-159, Doi 10.5194/Amt-5-149-2012, 2012.

928   Wolfe, G. M., and Thornton, J. A.: The chemistry of atmosphere-forest exchange (CAFE)
929   model - PART1: Model description and characterization, Atmos Chem Phys, 11,
930   77-101, 2011.

931   Wolfe, G. M., Crounse, J. D., Parrish, J. D., St Clair, J. M., Beaver, M. R., Paulot, F.,
932   Yoon, T. P., Wennberg, P. O., and Keutsch, F. N.: Photolysis, OH reactivity and
933   ozone reactivity of a proxy for isoprene-derived hydroperoxyenals (HPALDs),
934   Phys Chem Chem Phys, 14, 7276-7286, 2012.

935   Wolfe, G. M., Cantrell, C., Kim, S., Mauldin, R., Karl, T., Harley, P., Turnipseed, A.,
936   Zheng, W., Flocke, F., Apel, E., Hornbrook, R. S., Hall, S., Ullmann, K., Henry, S.
937   B., Digangi, J., Boyle, E. S., Kaser, L., Schnitzhofer, R., Hansel, A., Graus, M.,
938   Nakashima, Y., Kajii, Y., Guenther, A., and Keutsch, F.: Missing peroxy radical
939   sources within a rural forest canopy, Atmospheric Chemistry and Physics
940   Discussion, 13, 31713-31759, 2013.

941   Wong, K. W., Tsai, C., Lefer, B., Haman, C., Grossberg, N., Brune, W. H., Ren, X.,
942   Luke, W., and Stutz, J.: Daytime HONO vertical gradients during SHARP 2009 in
943   Houston, TX, Atmos Chem Phys, 12, 635-652, Doi 10.5194/Acp-12-635-2012,
944   2012.

945   Xing, J., Wang, S. X., Jang, C., Zhu, Y., and Hao, J. M.: Nonlinear response of ozone to
946   precursor emission changes in China: a modeling study using response surface
947   methodology, Atmos Chem Phys, 11, 5027-5044, Doi 10.5194/Acp-11-5027-2011,
948   2011.

949   Yoshino, A., Nakashima, Y., Miyazaki, K., Kato, S., Suthawaree, J., Shimo, N.,
950   Matsunaga, S., Chatani, S., Apel, E., Greenberg, J., Guenther, A., Ueno, H.,
951   Sasaki, H., Hoshi, J., Yokota, H., Ishii, K., and Kajii, Y.: Air quality diagnosis
952   from comprehensive observations of total OH reactivity and reactive trace species
953   in urban central Tokyo, Atmos Environ, 49, 51-59, Doi
954   10.1016/J.Atmosenv.2011.12.029, 2012.

955   Yuan, B., Warneke, C., Shao, M., and de Gouw, J. A.: Interpretation of volatile organic
956   compound measurements by proton-transfer-reaction mass spectrometry over the
957   deepwater horizon oil spill, International Journal of Mass Spectrometry, 358, 43-
958   48, Doi 10.1016/J.Ijms.2013.11.006, 2014.

959   Zhang, Y., Hu, X. M., Leung, L. R., and Gustafson, W. I.: Impacts of regional climate
960   change on biogenic emissions and air quality, J Geophys Res-Atmos, 113, Artn
961   D18310 Doi 10.1029/2008jd009965, 2008a.

962   Zhang, Y. H., Su, H., Zhong, L. J., Cheng, Y. F., Zeng, L. M., Wang, X. S., Xiang, Y. R.,
963   Wang, J. L., Gao, D. F., Shao, M., Fan, S. J., and Liu, S. C.: Regional ozone
964   pollution and observation-based approach for analyzing ozone-precursor
965   relationship during the PRIDE-PRD2004 campaign, Atmos Environ, 42, 6203-
966   6218, Doi 10.1016/J.Atmosenv.2008.05.002, 2008b.

967   Zhao, J., and Zhang, R. Y.: Proton transfer reaction rate constants between hydronium
968   ion (H_3O^+) and volatile organic compounds, Atmos Environ, 38, 2177-2185, 2004.

969   Zhou, X. L., Zhang, N., TerAvest, M., Tang, D., Hou, J., Bertman, S., Alaghmand, M.,
970   Shepson, P. B., Carroll, M. A., Griffith, S., Dusanter, S., and Stevens, P. S.: Nitric
971   acid photolysis on forest canopy surface as a source for tropospheric nitrous acid,
972   Nat Geosci, 4, 440-443, Doi 10.1038/Ngeo1164, 2011.

973
974

975

976   Table 1. Analytical characteristics of trace gas analyzers at TRF

977

Chemical Species	Manufacturer and Model Number	Uncertainty	Lower Limit of Detection
CO	Thermo Scientific 48i TLE	10%	40 ppb
NO_X	Thermo Scientific 42i-TL with a Mo-converter	15%	50 ppt
SO_2	Thermo Scientific 43i-TLE	10%	50 ppt
ozone	Thermo Scientific 49i	5%	< 1 ppb

978
979

980

981 Table 2. Terpenoid speciation analysis results from GC-MS a) branch enclosure and b)
982   ambient air samples.

983

984 a)

Terpenoids	*Composition(%)	Speciation	*Composition(%)
Isoprene	0.5		
Monoterpenes	92.9	α-pinene	36.7
		camphene	13.1
		β-pinene	12.0
		β-myrcene	27.7
		α-terpinolene	1.9
		d-limonene	8.6
Sesquiterpenes	6.6	β-caryophyllene	53.2
		α-caryophyllene	46.8

985

986 b)

Terpeniods	*Composition(%)	Speciation	*Composition(%)
Monoterpenes	98.6	α-pinene	38.8
		β-piene	36.5
		camphene	13.5
		d-limonene	11
Sesquiterpenes	1.4	longifolene	100

987 *Composition is calculated based on the mixing ratio scale

988
989

990

991

Table 3. A summary of critical differences in input parameters for four different model simulation scenarios presented in this study. The isoprene chemical scheme is based on Archibald et al. (2010a).

995

	HPALD chemistry	Observational Constraints
Scenario I	No	[-]All
Scenario II	[#]Peeters and Muller (2010)	[-]All
Scenario III	[+]Crounse et al. (2011)	[-]All
Scenario IV	No	[-]All but HONO

996

[#]k298 = ~ 0.08 for isoprene peroxy radical isomerization rate leading to produce HPALD, [+]k298 = 0.002 for isoprene peroxy radical isomerization rate, [-]All the observed diurnal variations, appeared in Figure 1 are constrained in the model along with ambient pressure and humidity.

1001
1002
1003
1004
1005
1006
1007
1008
1009
1010
1011
1012
1013
1014
1015
1016
1017

1018   Table 4 A summary for radical distributions from the observationally constrained box-
1019   model simulation results
1020

	OH		HO$_2$		RO$_2$		Constraints
Local Time	8:00-12:00	13:00-16:00	8:00-12:00	13:00-16:00	8:00-12:00	13:00-16:00	
Scenario I	3.85×10^6	3.08×10^6	4.10×10^8	7.02×10^8	3.65×10^8	1.14×10^9	All
Scenario II	3.99×10^6	3.69×10^6	3.99×10^8	7.86×10^8	3.51×10^8	9.62×10^8	All
Scenario III	3.86×10^6	3.13×10^6	4.09×10^8	7.09×10^8	3.64×10^8	1.12×10^9	All
Scenario IV	1.61×10^6	1.61×10^6	1.95×10^8	4.82×10^8	1.75×10^8	7.25×10^8	All but HONO

1021   unit: molecules cm^{-3}
1022
1023

1024 Figure 1. Averaged temporal variations observed trace gases and ambient temperature at
1025 TRF (June 1st to June 6th, 2012, KST stands for Korean Standard Time GMT+9). The
1026 uncertainty for each observable is listed in the main text.
1027
1028
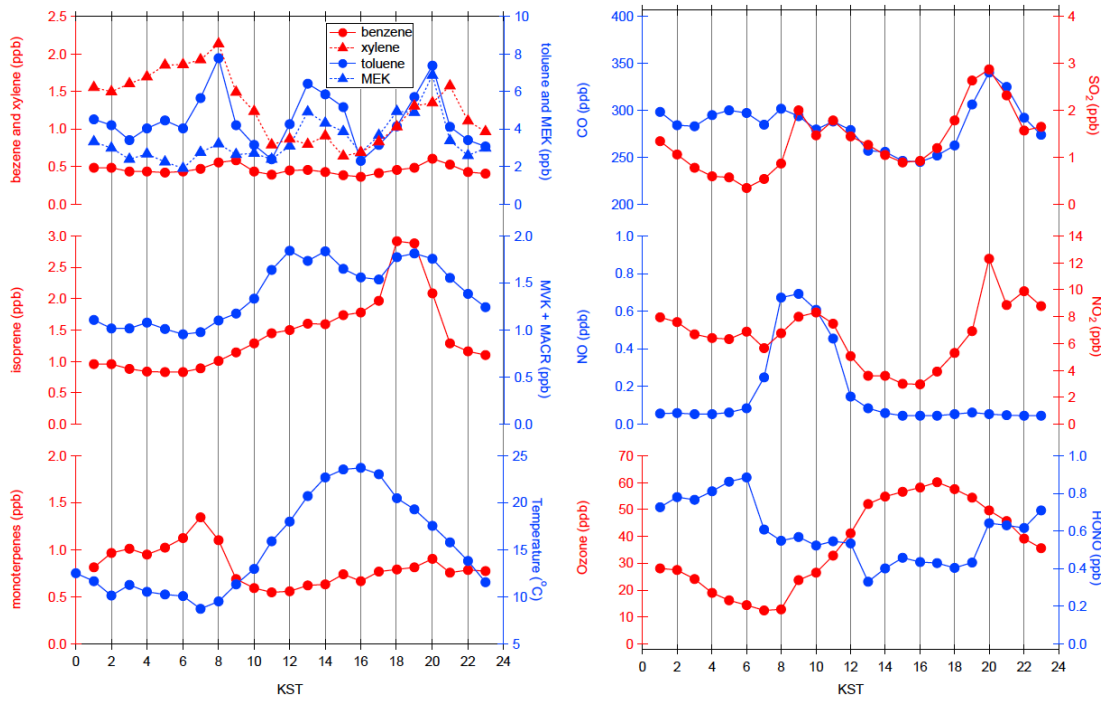
1029
1030
1031

1032   Figure 2. The temporal variations of OH reactivity calculated from the observed dataset
1033   at TRF (Figure 1).
1034
1035
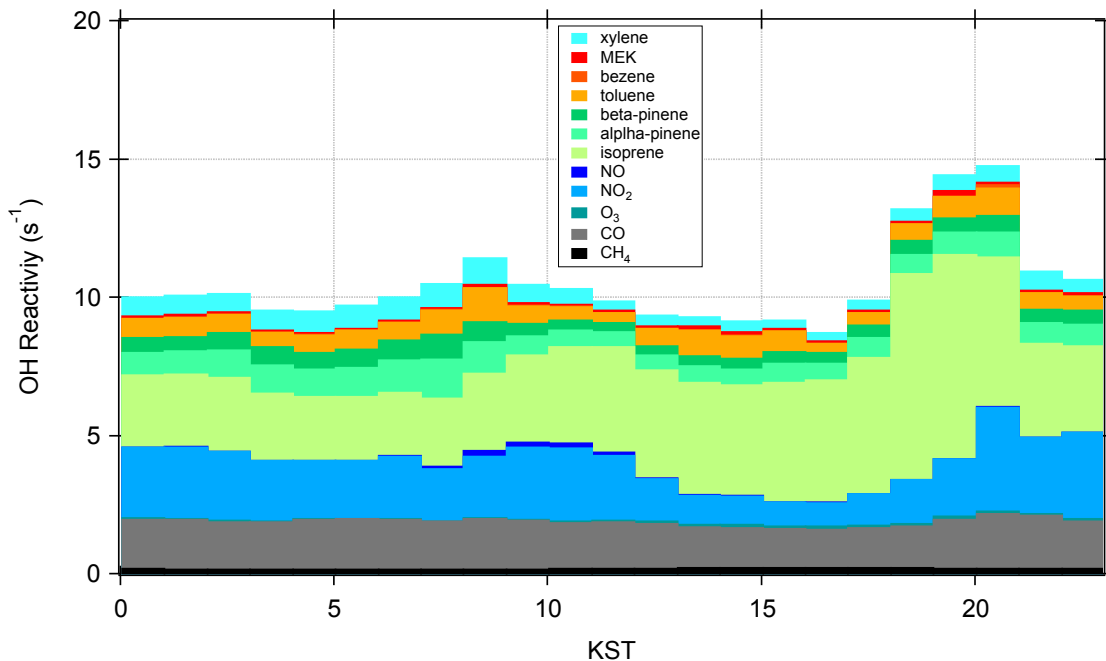
1036
1037
1038
1039

1040   Figure 3. The temporal variations of OH (a), HO_2 (b) , and RO_2 (c) calculated by four
1041   different observationally constrained UWCM box model scenarios.
1042

1043
1044
1045
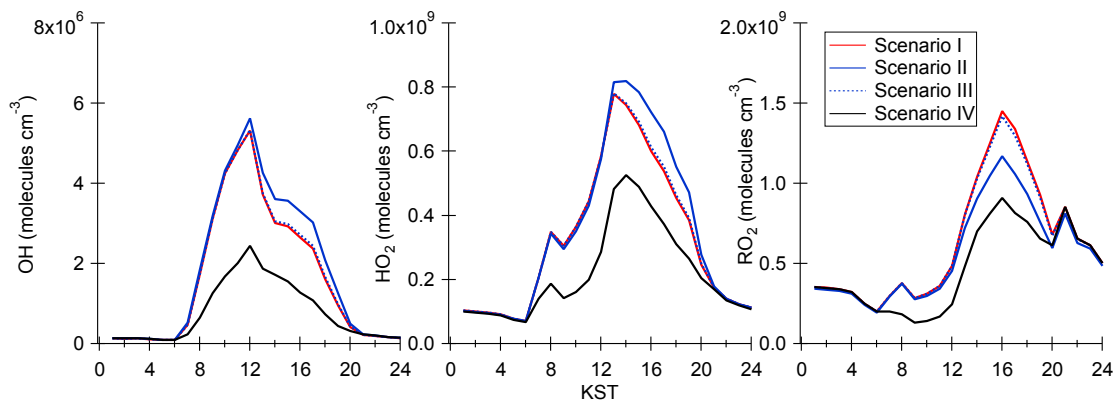
1046
1047 Figure 4 The temporal variations of radical recycling (red) and destruction (blue, black
1048 and green) rates calculated using the UWCM box model for different model scenarios
1049
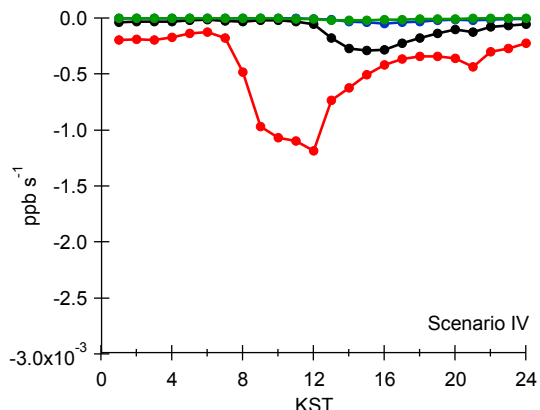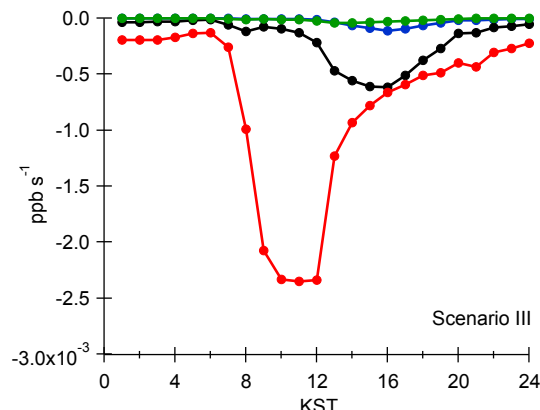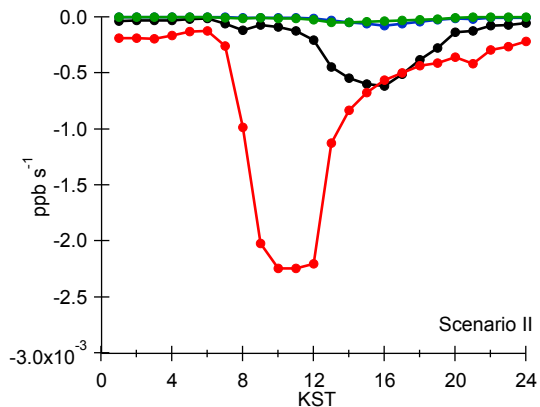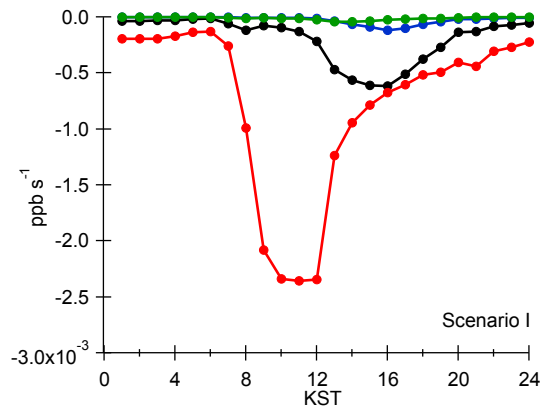
1050
1051
1052
1053
1054

Figure 5. The temporal variations of P_{H2O2}/P_{HNO3} calculated from the UWCM box model
from four different model scenarios
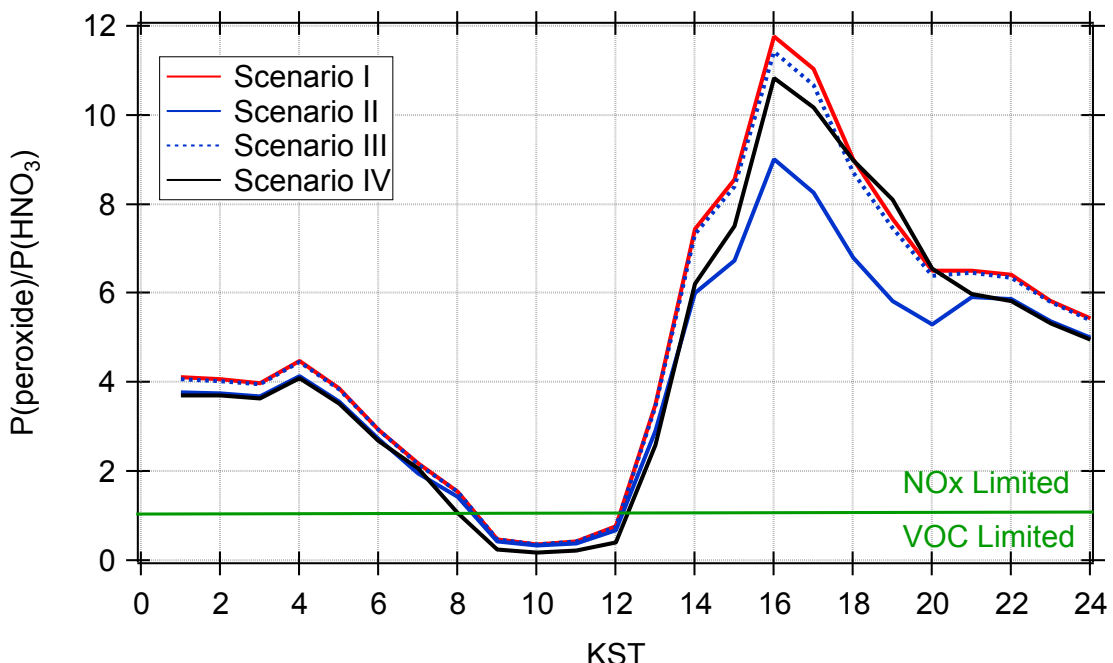
1062   Figure 6. The temporal distributions of UWCM calculated OH reactivity (a) and
1063   formaldehyde (b) from different model calculation scenarios

1064
1065
1066
1067